Pramana – J. Phys. (2017) 89:4
DOI 10.1007/s12043-017-1396-x

Structural and optical characteristics of Ce, Nd, Gd, and Dy-doped Al_2O_3 thin films

ASHWINI S VARPE and MRINALINI D DESHPANDE*

Department of Physics, H.P.T. Arts and R.Y.K. Science College, Nasik 422 005, India
*Corresponding author. E-mail: d_mrinal@yahoo.com

Published online 19 June 2017

Abstract. We present the optical properties of rare earth (RE)-doped Al_2O_3 thin films and discuss their possible use in applications like gate dielectric material and in coating industry. Aluminum oxide films doped with RE elements such as Ce, Nd, Gd, and Dy are synthesized on glass substrate using ultrasonic spray pyrolysis technique at 400°C. The concentration of rare earth element is varied from 0.5 to 5 mol% in 0.1 M solution of Al_2O_3. The X-ray diffraction analysis indicates that the thin films deposited with and without rare earth doping have an amorphous structure. Further, the optical properties of RE-doped Al_2O_3 thin films are studied by using UV–visible spectroscopy and photoluminescence measurement. The band gap is found to be 4.06 eV for Al_2O_3 thin film. A small blue shift is seen in the optical spectra of RE-doped samples as compared to undoped Al_2O_3 film. Dielectric constant of alumina thin film increases with doping of Gd and Dy while it decreases with Ce and Nd doping. Concentration quenching effects are observed in the photoluminescence spectra of Ce, Nd, Gd, and Dy-doped Al_2O_3 films. Among all these RE-doped Al_2O_3 thin films, Gd and Dy-doped Al_2O_3 films exhibit a potential for the construction of dielectric gate in transistors or as a coating material in the semiconductor industry.

Keywords. Aluminum oxide; optical properties; thin films; ultrasonic spray pyrolysis.

PACS Nos 78.20.−e; 81.15.Rs; 78.20.Ci

1. Introduction

Alumina, Al_2O_3, exhibits large band-gap energy (≈8.8 eV), excellent thermal stability, and higher dielectric constant (≈9) than SiO_2 (≈3.9) [1–3]. Al_2O_3 is considered to be one of the most attractive dielectric material due to its chemical and thermal stability, excellent dielectric properties and good silicon adhesion. Aluminum oxide thin films are used as gate dielectric films in electronic devices, encapsulation layers in light emitting diodes and antireflection coatings in solar thermal cells [4]. Al_2O_3 films can also be used as tunnelling barriers for magnetic tunnelling junctions (MTJ), magnetic random access memories (MRAM) [5], and extensions into other industrial areas such as corrosion-resistance and optical material coatings [6]. There are number of investigations related with Al_2O_3 films [7–13]. However, most of the studies have reported electrical and magnetic properties of Al_2O_3 thin films.

Alumina is a very good insulator with a high dielectric constant. These properties makes it useful for the semiconductor industry which constantly searches for new materials to build dielectric gate in transistors and coating materials in integrated circuits [1,6]. These properties can be further tuned by appropriate doping of the pure material. The doping should meet two basic criteria: (1) it must not drastically change the band gap of the pure material or the band offset around it and (2) at low energies, it must cause the increase in the dielectric constant. Theoretically [14] and experimentally [15], it is observed that although certain transition metals (TM) like Y, Sc, Zr, and Nb are present in aluminum oxide, only Y and Sc maintains the band-gap value with increase in dielectric constant of the host material. Among these TM elements, yttrium-doped α-Al_2O_3 may be one of the promising candidate in the development of semiconductors. RE-doped alumina is found to be a good luminescent material [16–22]. RE elements have a partially filled inner ($4f^n$) shell surrounded by completely filled outer ($5s^2$ and $5p^6$) orbitals. This results in the optical emission of very sharp lines at wavelengths from UV to IR [23,24]. Al_2O_3 employed as a matrix for rare-earth impurities such as Eu, Tb, and Ce showed excellent photoluminescence (PL) properties, with the emissions of red, green, and

blue colour, respectively [18–20]. Recently, Nd-doped Al_2O_3 films are characterized for the waveguide patterning [21]. Based on earlier studies, similar to the TM doping in alumina, it is interesting to exploit suitable RE element which will help to enhance the dielectric properties of alumina thin films with small variation in the band gap. Such investigation of the RE-doped aluminum oxide thin films has not yet been performed.

In the present study, we aim to engineer the band gap and dielectric properties of RE-doped alumina thin films by varying the RE concentration. Based on earlier studies [17,19–21], we have selected a few representative rare earth elements such as Ce, Nd, Gd, and Dy. We have deposited thin films by using ultrasonic spray pyrolysis technique. We have reported the optical properties, dielectric constant and refractive index of RE:Al_2O_3 thin films as a function of dopant concentration. It is observed that under ultraviolet excitation, Ce, Gd, and Dy-doped thin films show emissions in the visible region, while Nd:Al_2O_3 gives emissions in the IR region.

2. Methodology

Al_2O_3 and RE-doped Al_2O_3 thin films are prepared by ultrasonic spray pyrolysis technique using the starting solutions of aluminum chloride, cerium (Ce), neodymium (Nd), gadolinium (Gd), and dysprosium (Dy) nitrates. Based on earlier results [7,12,20], we have optimized the process for 0.1 M concentration of Al_2O_3. Our optimized parameters are as follows: the nozzle to substrate distance = 16 cm, flow rate = 7 ml/min, and spray time = 20 min. The glass substrate temperature is maintained at 400°C. The RE doping level is varied by changing the concentration of the RE element by 0.5, 1, 3, and 5 mol%. The structural properties of the films are studied by X-ray diffractometer (XRD)-Bruker D8 advance, Germany, using CuKα (λ = 1.54 Å) radiation. For thickness measurement of the thin films, we have used the spectroscopic reflectometer 100S model with TF Probe 2.4 software. Surface morphology and chemical composition are observed using a scanning electron microscope (SEM)-JEOL TSM-6360A with OXFORD and with energy dispersive spectroscopy (EDS) attachment. The optical absorption spectra is measured in the range 200–1000 nm using Shimadzu UV-2450 double beam spectrophotometer. From the optical spectra, we have calculated the band gap, dielectric constant, and refractive index. Photoluminescence measurements are carried out using a HORIBA JOBIN YVON fluoromax-4 spectrofluorometer at room temperature.

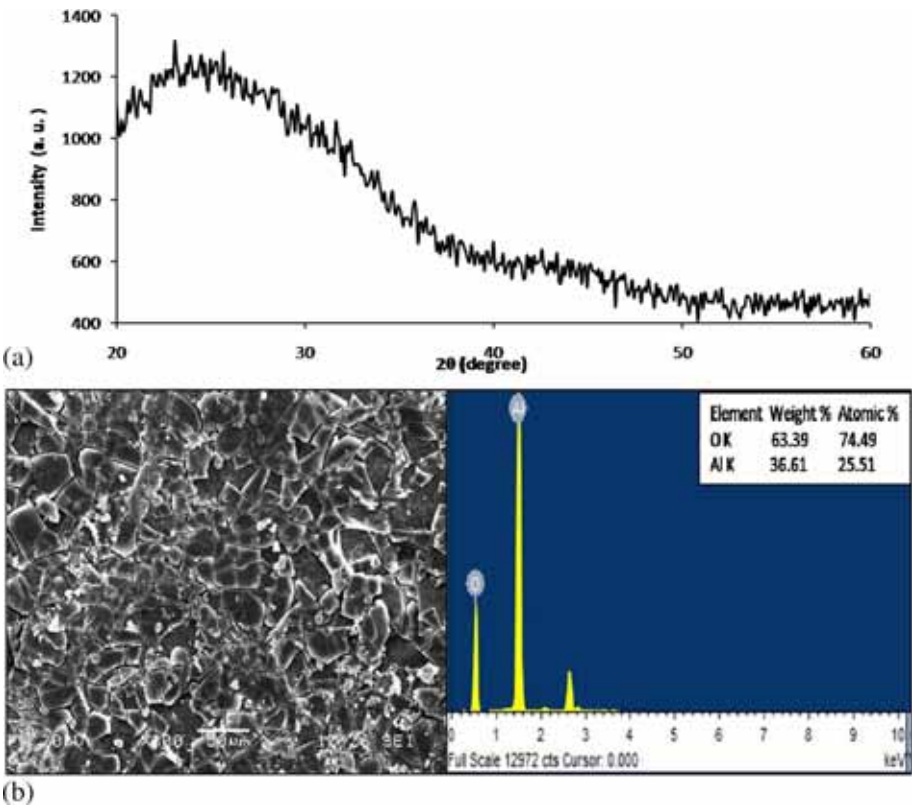

Figure 1. (**a**) XRD spectrum of Al_2O_3 thin film and (**b**) SEM micrograph and weight analysis via EDS spectrum of deposited Al_2O_3 thin film at 0.1 M concentration.

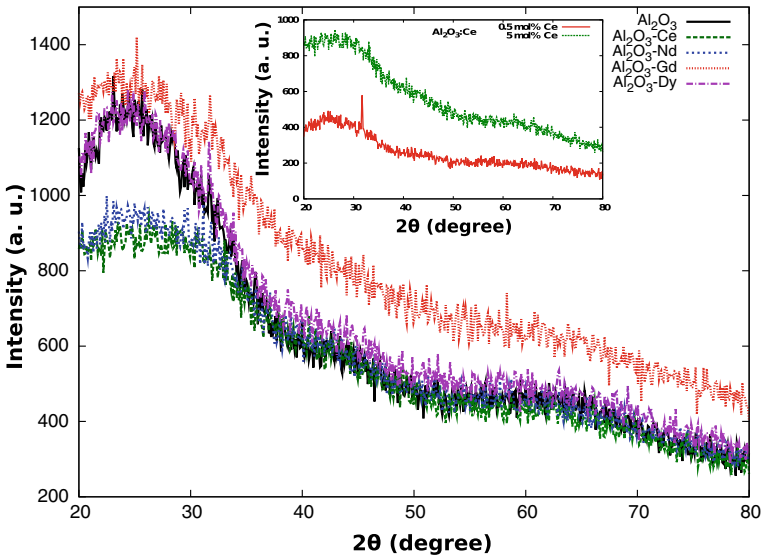

Figure 2. XRD patterns of RE:Al_2O_3 thin films for 5 mol% concentration of RE elements where RE = Ce, Nd, Gd, and Dy along with undoped Al_2O_3 thin film. The inset shows the XRD patterns of Ce-doped Al_2O_3 thin films for 0.5 and 5 mol% concentration of Ce.

3. Results and discussion

The XRD patterns of 0.1 M alumina thin film deposited on the glass substrate at temperature 400°C are presented in figure 1a. From the XRD pattern, it is seen that the prepared alumina thin film is amorphous in nature. It is accepted that alumina at temperatures below 600°C has an amorphous structure regardless of the deposition method [12]. Thickness of our prepared alumina thin film is in the range of 300−350 nm. The crack formation is observed via surface morphology analysis (figure 1b). The overall SEM analysis showed foamy agglomerated particles with a wide variation in the particle size. The particle size of the alumina thin film obtained from SEM is in the range of 4–15 nm. Sometimes, a little crack can be seen at the interface between the area coated with Al_2O_3 and the area which is not coated, because of heat change in the lattice during spray time. At high temperature, the stronger chemisorption causes much reduced adatom mobility and the resulting grain size becomes smaller. However, small clusters can coalesce by surface diffusion leading to agglomeration, and such agglomeration results in creating voids and discontinuities. The EDS confirms that there is an excess of oxygen in the film compared to the expected stoichiometry for Al_2O_3. This might be an indication for a low-density material.

For RE-doped alumina thin films, we have considered 0.5, 1, 3, and 5 mol% concentrations of RE elements. Figure 2 shows the evolution of X-ray diffraction patterns for the undoped and RE-doped Al_2O_3 thin films deposited on the glass substrate at 400°C. Here, we have shown the XRD patterns of Ce, Nd, Gd, and Dy-doped Al_2O_3 thin films for 5 mol% concentration of RE element. To show the concentration-dependent variations, in the inset of figure 2, we have shown the XRD patterns for Ce-doped Al_2O_3 films for 0.5 and 5 mol%, concentration. With the increase in concentration of Ce element, the peak intensity increases. From 0.5 to 5 mol%, similar trend is observed for Nd, Gd, and Dy. Similar to alumina thin film, XRD patterns of RE-doped alumina thin films show a very broad band without any indication of crystallinity. From the XRD patterns, it is seen that the peak intensity decreases with doping of Ce and Nd while for Gd and Dy, it increases as compared to that of Al_2O_3 thin films. These variations can be explained on the basis of difference in the radius between RE^{3+} ion and Al^{3+} ion. The ionic radii of Ce^{3+}, Nd^{3+}, Gd^{3+}, and Dy^{3+} are 1.07 Å, 1.04 Å, 0.97 Å, and 0.91 Å, respectively. The large difference in radius between Ce^{3+} (1.07 Å) and Al^{3+} (0.57 Å) may not lead to direct substitution and hence Ce^{3+} ions may be segregating to more energetically favourable grain boundary sites of the Al_2O_3 thin films. The increase in intensity observed with the concentration of Ce^{3+} ions is due to more segregation of Ce^{3+} ions along the grain boundary sites resulting in minimization of the surface energy. For all the RE elements, the increase in concentration results in increase in peak intensity of XRD pattern. But with the doping of large sized Ce^{3+} and Nd^{3+} ions, a decrease in intensity is observed in the XRD patterns compared to that of the undoped film. This reflects the more amorphous nature of the doped films. For Gd^{3+} and Dy^{3+} ions, the difference between ionic radii with respect to Al^{3+} decreases. The increase

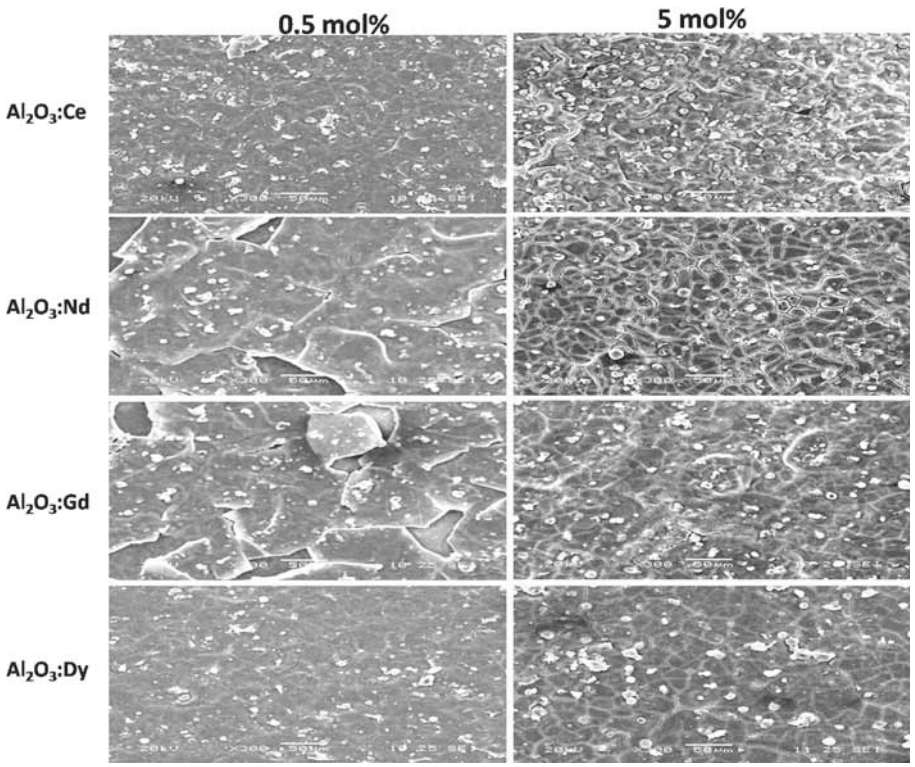

Figure 3. SEM micrographs for RE:Al_2O_3 thin films with RE = Ce, Nd, Gd, and Dy. The first and second columns represent the SEM micrographs for Ce, Nd, Gd, and Dy-doped Al_2O_3 thin films for 0.5 and 5 mol% concentration of RE element.

in peak intensities in the XRD patterns shows that substitution of Gd and Dy at the Al site is more favourable. The smaller size of Gd and Dy reduces the internal stress and surface energy in the host matrix leading to a decrease in the amorphous nature of the thin films.

Figure 3 shows the SEM images of RE-doped Al_2O_3 thin films for 0.5 and 5 mol% RE concentration. From the SEM images, it is seen that during the substitution of Al^{3+} with RE^{3+} ions at 5 mol% concentration, there is a substantial rearrangement of the nearest neighbour environment. It is observed that with the increase in concentration of RE elements, from Ce to Dy, the homogeneity of host thin film increases. Particle size and agglomeration of particles decrease from Ce to Dy. Overall, decrease in the density of grain boundaries may absorb or scatter the light generated inside the film which may result in lowering the photoluminescence brightness. Figure 4 represents the EDS pattern of RE-doped Al_2O_3 thin films. The patterns show that with increasing concentration of RE from 0.5 to 5 mol%, the effective doping of Ce, Nd, Gd, and Dy ions in alumina thin films. Separate peaks are observed for Gd and Dy-doped alumina thin films.

Table 1 lists the atomic percent elemental compositions of the RE, aluminum and oxygen concentrations in the pure and RE:Al_2O_3 thin films for 0.5 and 5 mol% of RE concentration in 0.1 M concentration of aluminum oxide thin films. Table 1 shows that the obtained thin film is composed of Al, O, and RE elements. Overall, for all the films the atomic ratio of oxygen to aluminium is over 3/2. The higher oxygen concentration shows the oxygen-rich nature of the deposited film.

To identify the suitability of RE-doped alumina thin films as a good dielectric material for the semiconductor industry, we have investigated the optical properties of RE-doped alumina thin films. Figure 5 shows the absorption spectra of RE:Al_2O_3 thin films at various concentrations of RE^{3+} ions. From the spectra, we have calculated the parameters such as band-gap energy (E_g), refractive index (n), extinction coefficient (k), and dielectric constant (ε) for undoped and RE-doped alumina thin films. From the absorption spectra (figure 5), it is seen that, the absorbance increases with increase in concentration of Ce, but decreases with the doping of Nd, Gd, and Dy in Al_2O_3 thin films. Absorbance of Ce shows broad spectra as compared to that of Nd, Gd and Dy-doped thin films. Substitution of Al^{3+} with large-sized Ce^{3+} generates more defects in Ce-doped alumina thin films. Due to the induction of defect levels, the number of transitions increases resulting in the broadening of absorption spectra. The overall absorption intensity decreases from Ce → Nd → Dy → Gd.

Figure 6 shows the variation of $(\alpha h\nu)^2$ vs. $h\nu$ (photon energy) for the deposited films. The optical band

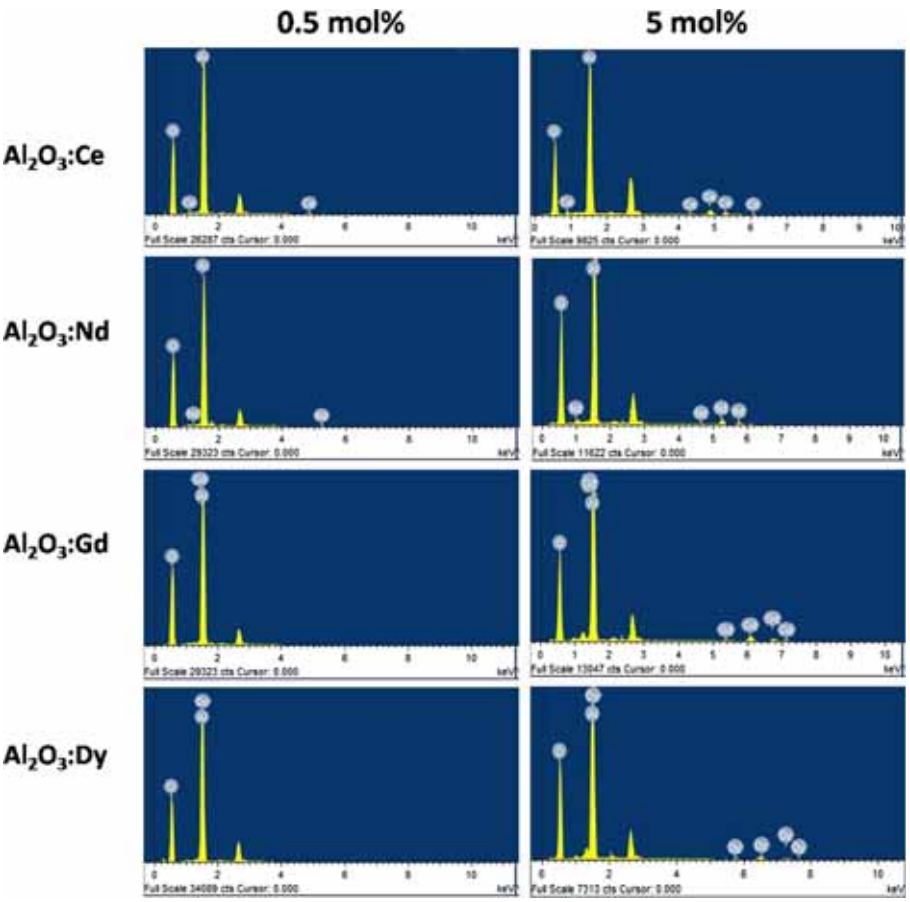

Figure 4. Elemental analysis via energy-dispersive spectroscopy for RE:Al_2O_3 thin films with RE = Ce, Nd, Gd, and Dy. The first and second columns represent the EDS for Ce, Nd, Gd, and Dy-doped Al_2O_3 thin films for 0.5 and 5 mol% concentration of RE element.

Table 1. Atomic percent elemental composition of the pure and RE:Al_2O_3 thin films as measured by EDS. The concentration of RE elements is 0.5 and 5mol% in 0.1 M aluminum oxide where RE = Ce, Nd, Gd, and Dy.

Sample	Al_2O_3	Al_2O_3:Ce		Al_2O_3:Nd		Al_2O_3:Gd		Al_2O_3:Dy	
RE%	–	0.5 mol%	5 mol%	0.5 mol%	5 mol%	0.5 mol%	5 mol%	0.5 mol%	5 mol%
RE	–	0.12	0.96	0.12	0.72	0.11	0 .98	0.11	0.67
O	74.49	76.48	77.46	77.02	79.12	77.42	77.08	76.33	77.62
Al	25.51	23.40	21.58	22.86	20.15	22.47	21.94	23.57	21.27
R (O/Al)	2.92	3.26	3.58	3.36	3.92	3.44	3.51	3.23	3.57

gap (E_g) is determined by extrapolating the linear part of the curves. The band gap of Al_2O_3 thin film for 0.1 M concentration is 4.06 eV. The reported band gap of amorphous alumina thin films by spray pyrolysis technique at 500°C is 3.92 eV [12]. For amorphous alumina and well-ordered alumina thin films deposited by various techniques, the band-gap energies are in the range of 3.2–5.5 eV [12,13], The band gap of the bulk alumina has a value 8.7 eV [10]. The decrease in band gap with respect to bulk value as well as compare to the crystalline thin films is associated with defect-induced states located in the band gap. Small blue shift in the spectra reflects the increase in the band gap of RE-doped thin film. Table 2 shows the overall increase in band gap for RE-doped sample as compared to pure alumina. The small increase in the band gap reflects the enhanced stability of these thin films.

Optical constants (i.e. refractive index and extinction coefficient) are the parameters which characterize how a material responds to an electromagnetic field. In the present study, the absorption coefficient (α), refractive

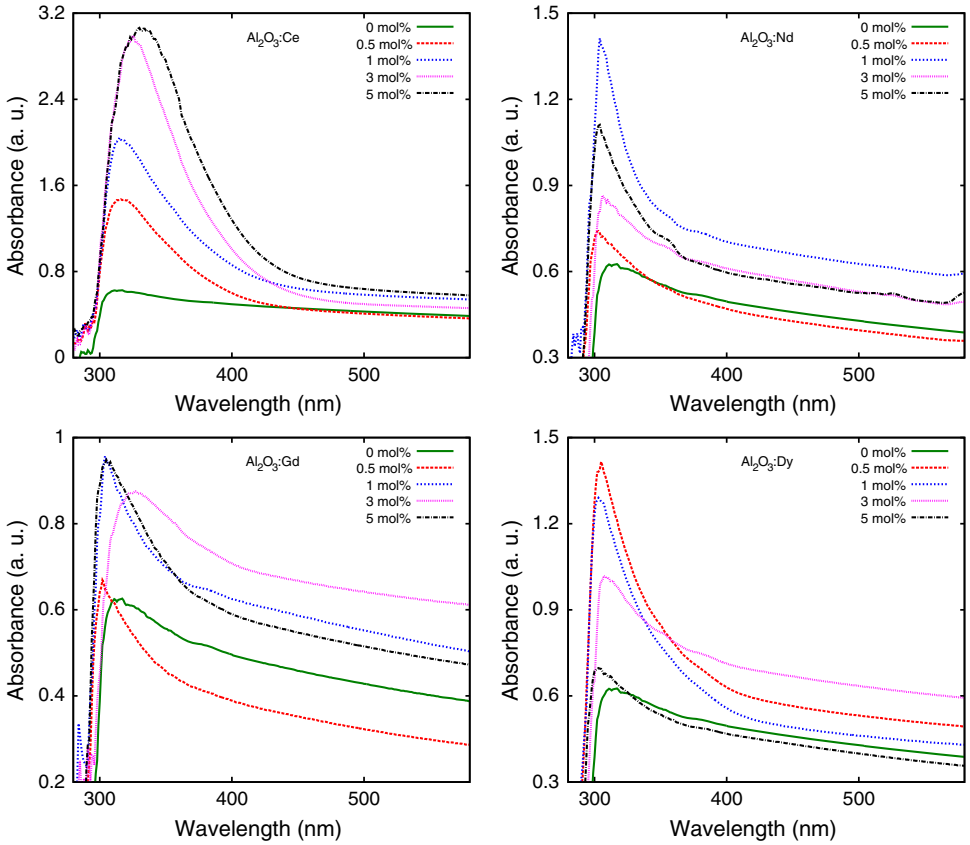

Figure 5. Absorption spectra of pure and RE:Al_2O_3 thin films with various concentrations of RE, where RE = Ce, Nd, Gd, and Dy.

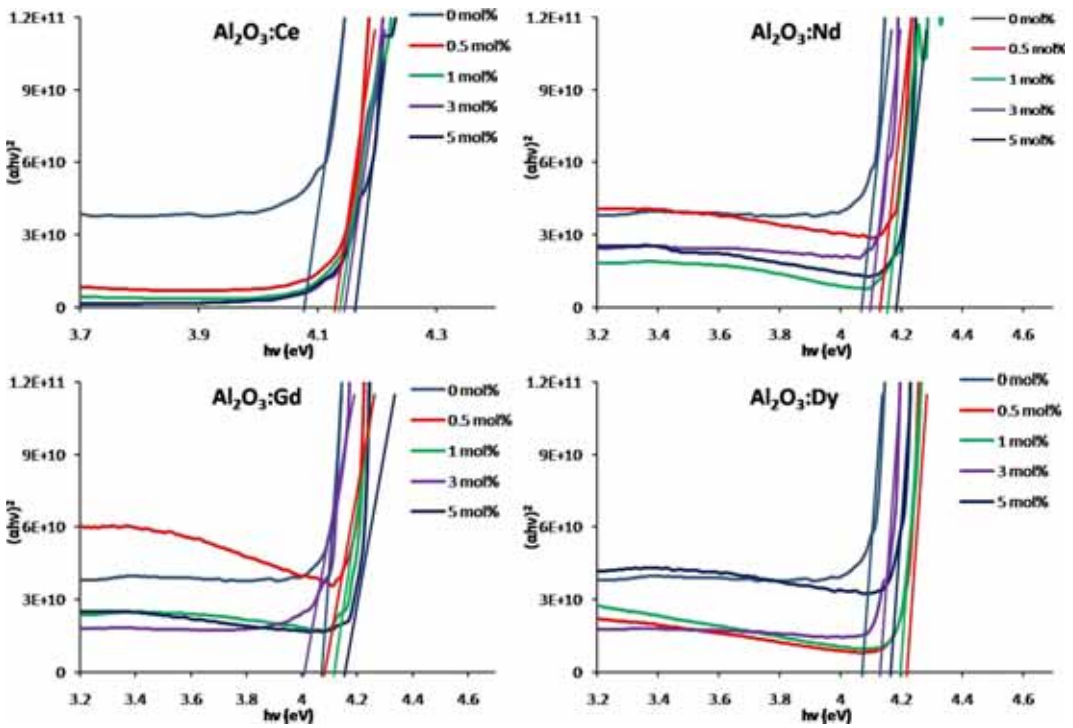

Figure 6. Plots of $(\alpha h\nu)^2$ vs. $(h\nu)$ for pure and RE:Al_2O_3 thin films with various concentrations of RE, where RE = Ce, Nd, Gd, and Dy.

Table 2. Band-gap energy (eV) of RE:Al_2O_3 thin films with various concentrations of RE, where RE = Ce, Nd, Gd, and Dy.

Sample	0 mol%	0.5 mol%	1 mol%	3 mol%	5 mol%
Ce:Al_2O_3	4.06	4.12	4.11	4.14	4.16
Nd:Al_2O_3	4.06	4.17	4.22	4.12	4.20
Gd:Al_2O_3	4.06	4.10	4.17	4.09	4.19
Dy:Al_2O_3	4.06	4.11	4.21	4.20	4.15

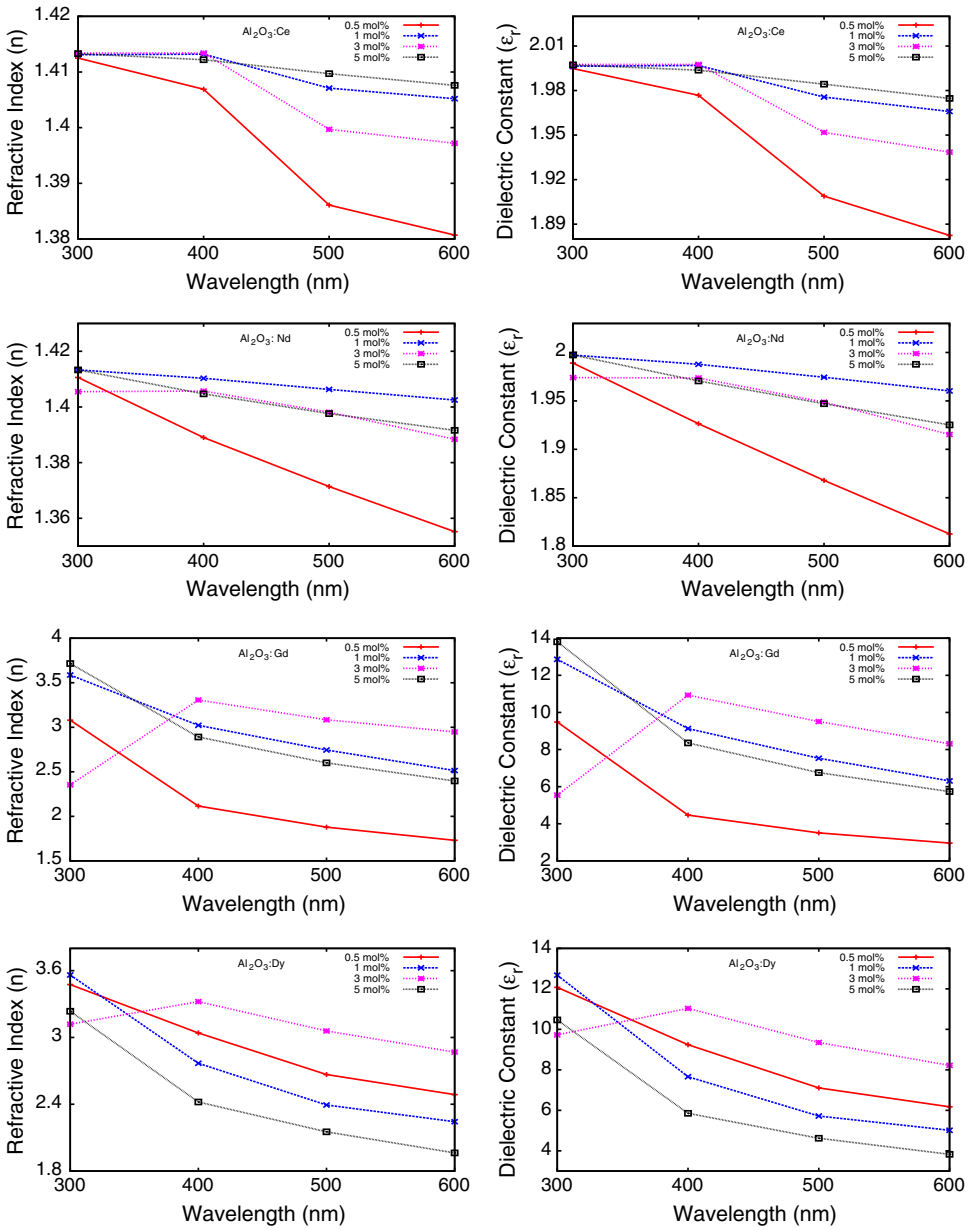

Figure 7. Refractive index (1st column) and dielectric constant (2nd column) of RE:Al_2O_3 thin films with various concentrations of RE elements, where RE = Ce, Nd, Gd, and Dy.

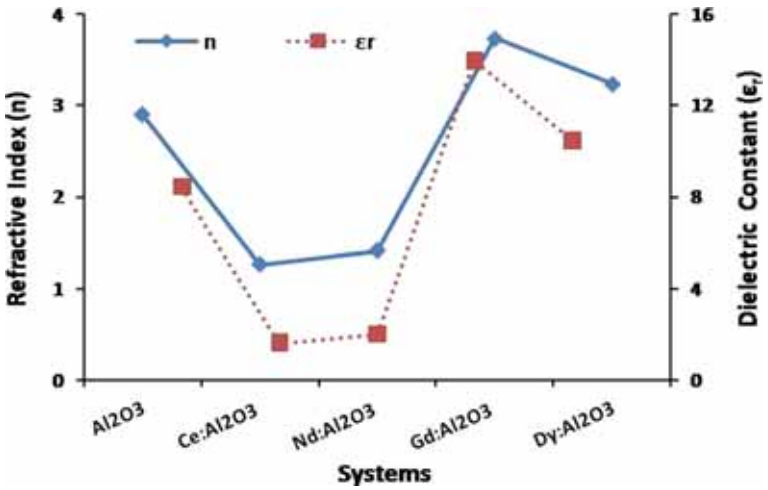

Figure 8. Variations of refractive index and dielectric constant of Al_2O_3 and RE:Al_2O_3 thin films at 5 mol% of RE, where RE = Ce, Nd, Gd, and Dy.

index (n), extinction coefficient (k), and dielectric constant (ε) of the films have been calculated by using the following formulae [25]:

$$\alpha = \frac{1}{d}\ln\left(\frac{1}{T}\right), \tag{1}$$

where α is the absorption coefficient, d and T are the thickness and transmittance of the film, respectively. The reflectance R of the material with transmittance (T) and absorbance (A) is given by the relation

$$R = 1 - (Te^{A})^2. \tag{2}$$

The refractive index (n) and extinction coefficient (k) of the film are calculated from the equations

$$n = \frac{(1+R)}{(1-R)} + \left[\frac{4R}{(1-R)^2} - k^2\right]^{1/2}, \quad k = \alpha\lambda/4\pi. \tag{3}$$

The complex dielectric constant is described as the sum of the real component (ε_r) and imaginary component (ε_i).

$$\varepsilon = \varepsilon_r + \varepsilon_i \quad \text{where} \quad \varepsilon_r = n^2 - k^2 \quad \text{and} \quad \varepsilon_i = 2nk. \tag{4}$$

In figure 7, we have plotted the refractive index and real component of the dielectric constant of RE-doped alumina thin films. In the present study, the refractive index and dielectric constant of pure alumina thin film at 0.1 M concentration are 2.10 and 8.4, respectively. From the earlier studies [7,12], it is observed that the refractive indices of Al_2O_3 thin films are in the range of 1.66 to 2.62. The refractive index and dielectric constant smoothly decreases with increasing wavelength. This decrease in the refractive index can be associated with fundamental band-gap absorption. The lower values of extinction coefficient reflect the absorption of electromagnetic waves due to inelastic scattering events [12].

With the RE doping, the calculated refractive index of the prepared alumina thin films are in the range of 1.41–3.71 at the maximum peak wavelength. The dielectric constants vary in the range of 1.99–14.31. Figure 8 shows the variation in refractive index and dielectric constant for RE-doped Al_2O_3 thin films at 5 mol% Ce, Nd, Gd, and Dy. Compared to pure alumina thin film, at 5 mol% concentration of RE elements, the refractive index and dielectric constant decrease from Ce to Nd but with Gd and Dy doping, it increases. The decrease in refractive index can be correlated with the variation in the microstructure observed via SEM. The smaller particle size causes multiple reflection of light at the grain boundary leading to a decrease in refractive index. Overall, it is seen that among Ce, Nd, Gd, and Dy elements, Gd:Al_2O_3 and Dy:Al_2O_3 thin films have high dielectric constants and small band offsets compared to the host thin film. As we compare the variations in the band gap and dielectric constant for RE:Al_2O_3 thin films with Al_2O_3 thin films, it is observed that Gd and Dy-doped alumina thin films are promising candidates for replacement of SiO_2.

To understand the luminescence properties, we have characterized the photoluminescence spectra of undoped and RE-doped Al_2O_3 thin films. Figure 9 shows the photoluminescence spectra of pure and Ce, Nd, Gd, and Dy-doped Al_2O_3 thin films at 0.5, 1, 3, and 5 mol% of RE concentration. To characterize the PL of alumina thin film, we have used an excitation wavelength of 300 nm. For Ce, Nd, Gd, and Dy-doped films, the excitation wavelength is 290, 800, 275, and 350 nm, respectively. For Al_2O_3 film, the peak positions in the PL spectra are at 400, 469, and 562 nm wavelength. These transitions are attributed to the visible region. Our calculated PL spectra of alumina thin film is consistent with PL spectra reported by Pustovarov

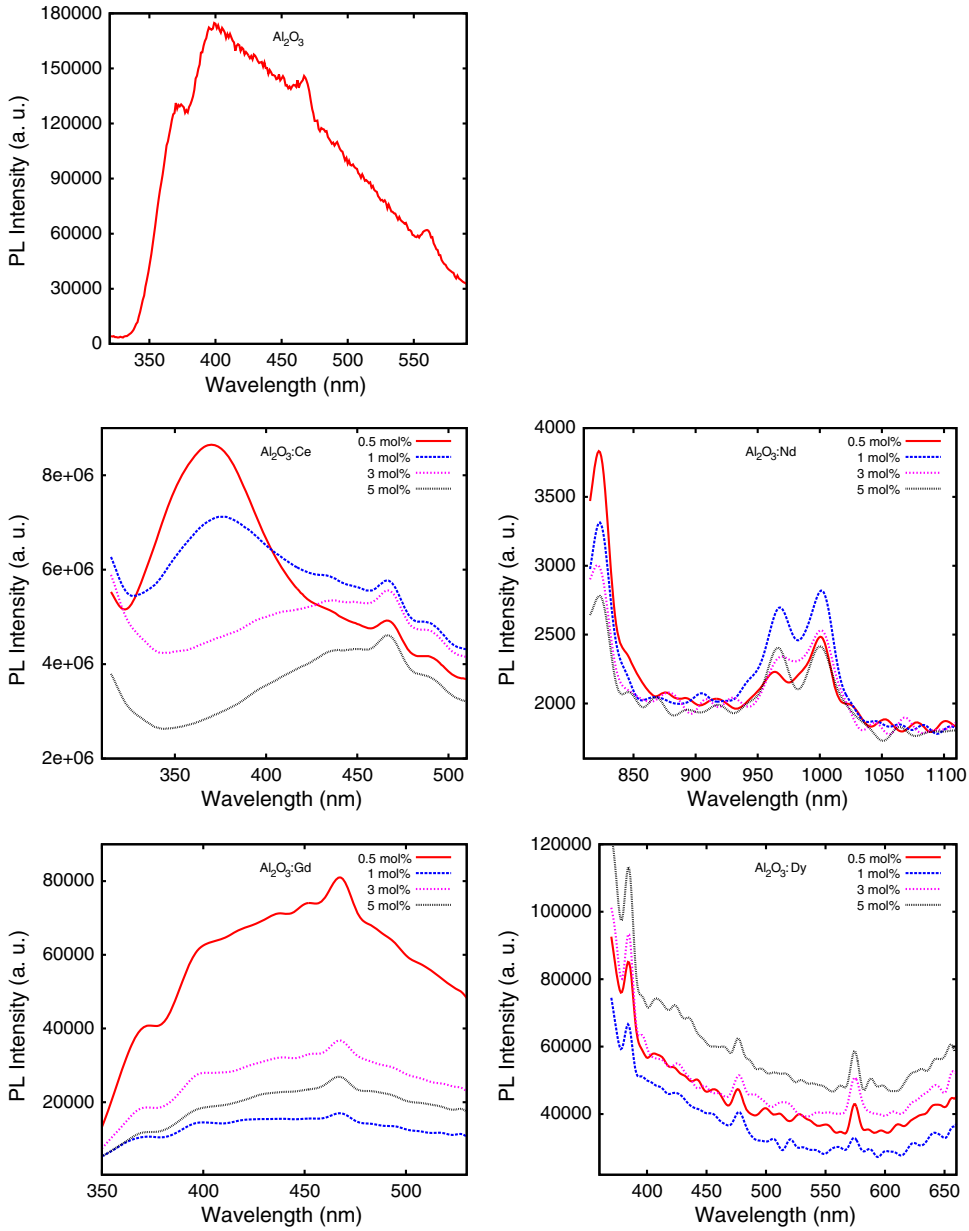

Figure 9. Photoluminescence spectra of pure and RE:Al_2O_3 thin films with 0.5, 1, 3, and 5 mol% concentration of RE-doped Al_2O_3 thin film where, RE = Ce, Nd, Gd, and Dy.

et al [10]. The emission peak around 400 nm wavelength confirms the oxygen vacancies in the film [10]. From the PL spectra, it is observed that PL intensity of host thin film increases with Ce doping and decreases in Nd, Gd and Dy-doped films. The concentration-dependent variations in the PL spectra are evidently observed.

The luminescence peaks in Ce-doped alumina thin films are broad and they are located approximately around 371, 468, and 483 nm wavelength. The blue broad band (468 and 483 nm) is associated with strong inhomogeneous broadening due to the amorphous structure of these thin films. Earlier studies [19,20] have shown that, for Ce:Al_2O_3 thin films, for 2 mol% concentration of Ce, the broad band is associated with interlevel transitions of the electronic energy states of Ce^{3+}. The blue emission can be attributed to the de-excitation of Ce^{3+} ions from the $^2D_{3/2}$ excited state to the split ground state into their $^2F_{7/2}$ and $^2F_{5/2}$ components [20]. Even though the enhanced PL intensity is observed for Ce:Al_2O_3 as compared to that of host thin film further, it is observed that with the increase in concentration of Ce^{3+} from 0.5 to 5 mol%, the intensity of PL spectrum decreases. At higher concentration of Ce, the decrease in PL intensity may be due to the cross relaxation between Ce^{3+} ions. It is

observed in SEM images that with increase in doping concentration of Ce, homogeneity of the doped film decreases. By increasing the grain size, the density of grain boundaries decreases. Furthermore, these grain boundaries may absorb or scatter the light generated inside the film resulting in lower PL brightness at higher concentration.

The PL intensity of the Al_2O_3 thin film decreases with Nd^{3+} doping. Similar to Ce:Al_2O_3, concentration quenching effect in PL intensity is observed for Nd:Al_2O_3 thin films. The PL intensity decreases from 0.5 to 5 mol%. Nd^{3+}-doped Al_2O_3 films are excited with 800 nm wavelength that is resonant with $^4I_{9/2} \rightarrow {}^2H_{9/2}$. Three sharp peaks are observed approximately at 823, 970, and 1004 nm wavelength which are in the IR region. The excited $^2H_{9/2}$ decays non-radiatively into $^4F_{3/2}$ state and gives three emission bands $^4F_{3/2} \rightarrow {}^4I_{9/2}$, $^4I_{11/2}$ and $^4I_{15/2}$. Ishizaka *et al* [16] have also shown that, at various concentrations of Nd^{3+} in alumina thin films, the emissions are observed near the IR region.

In the PL spectra of Gd:Al_2O_3 thin films, it is seen that for various concentration of Gd in Al_2O_3, single emission peak is observed at 468 nm wavelength. This peak may be due to deep level or trap-state emission in visible region, and it corresponds to the ionized oxygen vacancies in the Gd:Al_2O_3 thin films [17]. The reduction in PL peak intensity after doping is attributed to the filling of oxygen vacancies, which is responsible for the blue emission ($^6P_{7/2} \rightarrow {}^8S_{7/2}$). The PL intensity is highest for 0.5 mol% concentration and decreases for 3, 5, and 1 mol% of Gd:Al_2O_3 thin films.

In the emission spectra of Dy:Al_2O_3, the dominant emission peaks are observed at 375, 385 (violet), 478 (blue), 576 (yellow), and 668 nm (red) wavelength. These different emission bands are originated from the same excitation wavelength (350 nm). The emission peak at 375 nm wavelength is in the ultraviolet region whereas others are in the visible region. The emissions around 478, 576, and 668 nm are due to the transition of $^4F_{9/2} \rightarrow {}^6H_{15/2}$, $^6H_{13/2}$, and $^6H_{11/2}$ [24]. It can be seen that for 0.5, 3, and 5 mol% of Dy^{3+} in Al_2O_3 thin film, the emission intensity of PL spectra increases except for 1 mol%.

Due to lower concentration of aluminum oxide as well as RE, concentration-dependent quenching effects are dominantly observed. It is found that after doping Gd and Dy in alumina thin films, the refractive index and dielectric constant of Al_2O_3 thin film increases with a small variation in band gap. Gd and Dy-doped Al_2O_3 thin films can serve as potential candidates for the construction of dielectric gate in transistors.

4. Conclusions

Al_2O_3 and RE-doped Al_2O_3 thin films are successfully deposited on glass substrate by ultrasonic spray pyrolysis technique at 400°C. The structural, morphological, and optical properties have been investigated for 0.1 M solution of Al_2O_3 and RE-doped Al_2O_3 thin films where RE = Ce, Nd, Gd, and Dy. The concentration of RE is varied from 0.5 to 5 mol%. XRD pattern shows the amorphous nature of all the samples. Thickness of all the prepared thin films is in the range of 300–350 nm. Absorption and photoluminescence results are more informative compared to XRD and SEM. The band-gap energy of Al_2O_3 thin film for 0.1 M concentration is 4.06 eV. The overall band gap of Al_2O_3 thin films increases with the increase in concentration of RE. Hence, blue shift is observed in the optical spectra. The refractive index and dielectric constant of Al_2O_3 thin film are 2.10 and 8.4, respectively. From the optical properties, it is found that among Ce, Nd, Gd, and Dy doping in Al_2O_3 thin film, only Gd and Dy enhance the dielectric constant of Al_2O_3 thin films with small variation in the band gap. Among these elements, Gd and Dy can serve as potential candidates for the construction of dielectric gate in transistors in semiconductor industry. Under ultraviolet excitation, Ce, Gd, and Dy-doped thin films show emissions in the visible region while Nd:Al_2O_3 shows emissions in the IR region. The optical properties demonstrated by the films under different doping concentrations offered the possibility in application as a gate dielectric material and in coating industry. However, further investigation and optimization still need to be done for RE:Al_2O_3 films.

Acknowledgements

MDD and AV acknowledge S.P. University of Pune, North Maharashtra University (NMU), Jalgaon and Department of Chemistry, H.P.T. Arts and R.Y.K. Science College, Nasik, for providing experimental facilities.

References

[1] J Koo, S Kim, S Jeon and H Jeon, *J. Korean Phys. Soc.* **48**, 131 (2006)
[2] S Choi, J Koo, Y Kim and H Jeon, *J. Korean Phys. Soc.* **46**, 945 (2005)
[3] S K Kim and C S Hwang, *J. Appl. Phys.* **96**, 2323 (2004)
[4] G N van den Hoven, E Snoeks, A Polman, J W M van Uffelen, Y S Oei and M K Smit, *Appl. Phys. Lett.* **62**, 3065 (1993)

[5] K I Lee, J H Lee, W Y Lee, K W Rhie, J G Ha, C S Kim and K H Shin, *J. Magn. Magn. Mater.* **239**, 120 (2002)
[6] D Riihela, M Ritala, R Materoa and M Leskela, *Thin Solid Films* **289**, 250 (1996)
[7] Z-Y Wang, R-J Zhang, H-L Lu, X Chen, Y Sun, Y Zhang, Y-F Wei, J-P Xu, S-Y Wang, Y-X Zheng and L-Y Chen, *Nano. Res. Lett.* **10**, 46 (2015)
[8] B P Dhonge, T Mathews, S T Sundari, R Krishan, A K Balamurugan, M Kamruddin, R V Subbarao, S Dash and A K Tyagi, Appl. Surf. Sci. 265, 257 (2013).
[9] P Kumar, M Wiedmann, C H Winter and I Avrutsky, *Opt. Soc. Am.* **48**, 5407 (2009)
[10] V A Pustovarov, V S Aliev, T V Perevalov, V A Gritsenko and A P Eliseev, *J. Exp. Theoret. Phys.* **111**, 989 (2010)
[11] B Lux, C Colombier and H Altena, *Thin Solid Films* **138**, 49 (1986)
[12] A B Khatibani and S M Rozati, *Mater. Sci. Semi. Proc.* **18**, 80 (2014)
[13] I Costina and R Franchy, *Appl. Phys. Lett.* **78**, 4139 (2001)
[14] M Haverty, A Kawamoto, K Cho and R Dutton, *Appl. Phys. Lett.* **80**, 2669 (2002)
[15] R Jung, J C Lee, Y W So, T W Noh, S J So and H J Shin, *Appl. Phys. Lett*. **83**, 5226 (2003)
[16] T Ishizaka, Y Kurokawa, T Makino and Y Segawa, *Opt. Mater.* **15**, 293 (2001)
[17] T Ishizaka and Y Kurokawa, *J. Lumin.* **92**, 57 (2001)
[18] R Marteinez-Martinez, J Rickards, M Garcia-Hipolito, R Trejo-Luna, E Martinez-Sanchez, O Alvarez-Fregoso, F Ramos-Brito and C Falcony, *Nucl. Instrum. Methods Phys. Res. B* **241**, 450 (2005)
[19] S Carmona-Tellez, C Falcony, M Aguilar-Frutis, G Alarcon-Flores, M Garcia-Hipolito and R Martinez-Martinez, *ECS J. Solid State Sci. Tech.* **2**, R111 (2013)
[20] R Martinez-Martinez, M Garcia-Hipolito, F Ramos-Brito, J L Hernandez-Pozos, U Caldino and C Falcony, *J. Phys.: Condens. Matter* **17**, 3647 (2005)
[21] A G Okhrimchuk, A I Krikunov, Y A Obod and O D Volplan, *J. Laser Micro/Nanoeng.* **10**, 124 (2015)
[22] S Gravani, K Polychronopoulou, V Stolojan, Q Cui, P N Gibson, S J Hinder, Z Gu, C C Doumanidis, M A Baker and C Rebholz, *Nanotechnol.* **21**, 465606 (2010)
[23] A E Esparza Garcia, M Garcia, C Falcony and J Azorin Nieto, *Superficies y Vacio* **11**, 80 (2000)
[24] V B Pawade and S J Dhoble, *J. Lumin.* **145**, 626 (2014)
[25] S Aydogu, O Sendil and M B Coban, *Chin. J. Phys.* **50**, 89 (2012)